What happens when a dopant doesn't go where you expect it to go? The case of MBE-grown Yb-doped $SrTiO_3$ on Si(001)

S. A. Chambers[1], E. Ramerez[2], D. Guragain[2], J. H. Ngai[2], P. V. Sushko[1], K. P. Koirala[1], Y. Du[1], N. Govind[1], M.E. Bowden[1], D. Biswas[3], T.-L. Lee[3], C. Weiland[4], J. C. Woicik[4]

[1]Physical Sciences Division, Physical and Computational Sciences Directorate, Pacific Northwest National Laboratory, Richland, WA 99352, USA
[2]Department of Physics, University of Texas-Arlington, Arlington, TX 76019, USA
[3]Diamond Light Source, Harwell Science and Innovation Campus, Didcot, England, UK
[4]National Institute of Standards and Technology, Gaithersburg, MD 20899, USA

We present the structural and electronic properties of Yb-doped $SrTiO_3$/Si(001) grown by molecular beam epitaxy. Other rare-earth dopants that result in *n*-type conductivity in the ABO_3 perovskite lattice typically substitute for Sr at the *A*-sites. In contrast, Yb is shown to substitute predominantly for Ti at the perovskite *B*-sites based on data from atomically resolved scanning transmission electron microscopy and energy dispersive spectroscopy, as well as extended x-ray absorption fine structure measurements. An atom beam flux (Θ) mismatch was present during film deposition because it was *assumed* that Yb would occupy *A*-sites. As a result, the fluxes were set such that $\Theta_{Yb} + \Theta_{Sr} = \Theta_{Ti}$. The formation of Yb_{Ti} rather than Yb_{Sr} results in Sr vacancies and extraneous (i.e. non-lattice) Ti atoms in the films. Yb exhibits two distinct charge states as determined by x-ray absorption spectroscopy and associated theoretical modeling, +2.7 and +2.1. These aliovalent dopants are compensated by donor electrons from oxygen vacancies that form during epitaxial film growth. The defect complexes resulting from the flux mismatch, together with oxygen vacancies, lead to deep-level electron traps that were detected by resonant photoemission and predicted to be stable by *ab initio* theory, as well as much higher sheet resistance than that associated with, for instance, La-doped $SrTiO_3$ films. *Ab initio* calculations show that the preference for *B*-site occupancy is driven by low oxygen chemical potential at the growth front as required to successfully deposit epitaxial STO on Si without amorphous SiO_2 formation at the interface.

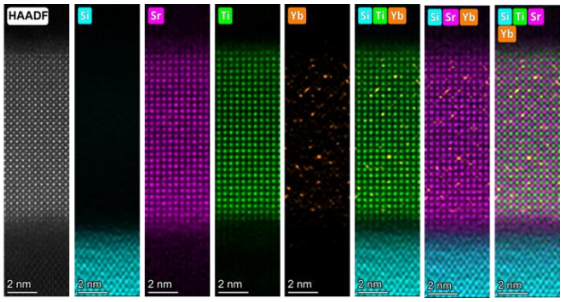

FIG. 1 TEM HAADF and EDS maps for 12 nm $(Yb_{0.03},V_O):Sr_{0.97}TiO_{3-\delta}/i$-Si(001). The Yb EDS map reveals that the dopant atoms are well dispersed. Visual inspection reveals that of the ~26 Yb atomic sites revealed in the Yb map, 22 overlap with Ti sites and 4 overlap with Sr sites.

[+] Author for correspondence: sa.chambers@pnnl.gov

Supplementary Information

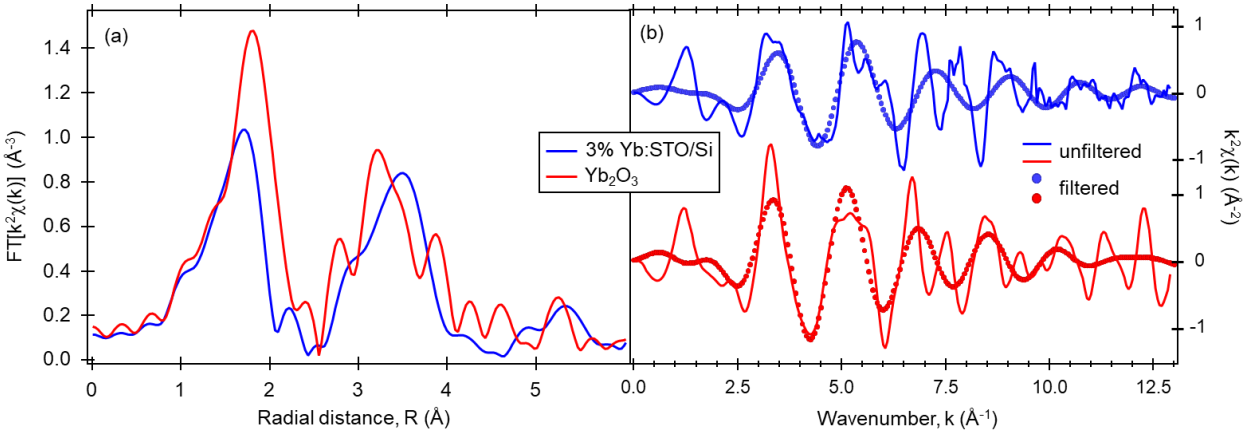

FIG. 2 (a) Fourier transforms of the k^2-weighted Yb L_3-edge EXAFS for 12 nm $(Yb_{0.03},V_O):Sr_{0.97}TiO_{3-\delta}$/*i*-Si(001) and polycrystalline Yb_2O_3 powder. (b) As-measured and Fourier filtered first-shell contributions corresponding to the first-neighbor Yb-O bond length. Note the lower frequency of the EXAFS oscillations for Yb:STO compared to Yb_2O_3, indicating a shorter Yb-O bond length in Yb:STO. This result suggests that Yb occupies *B*-sites because the *B*-O bond length in STO (1.953 Å) is considerably shorter than that for the *A*-O bond (2.761 Å).

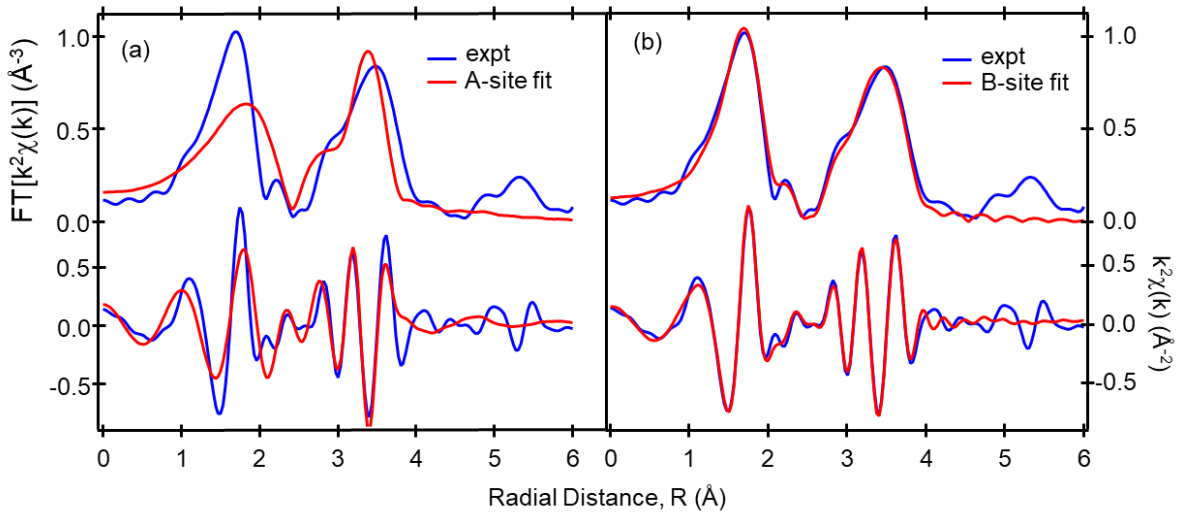

FIG 3 Best fits of the k^2-weighted Yb L_3-edge EXAFS data for 12 nm $(Yb_{0.03},V_O):Sr_{0.97}TiO_{3-\delta}$/*i*-Si(001) assuming Yb substitution for (a) Sr at the A-sites and (b) Ti at the B-sites in the STO lattice. The upper portion of each panel shows the forward Fourier transform and the bottom portions show the back-Fourier transform of the data, together with their fits. The fits include the first three single-scattering paths for each substitutional site. A site - Yb-O, Yb-Ti, and Yb-Sr. B site - Yb-O, Yb-Sr, and Yb-Ti. The fit to the *B*-site model is clearly superior to that for the *A*-site model.

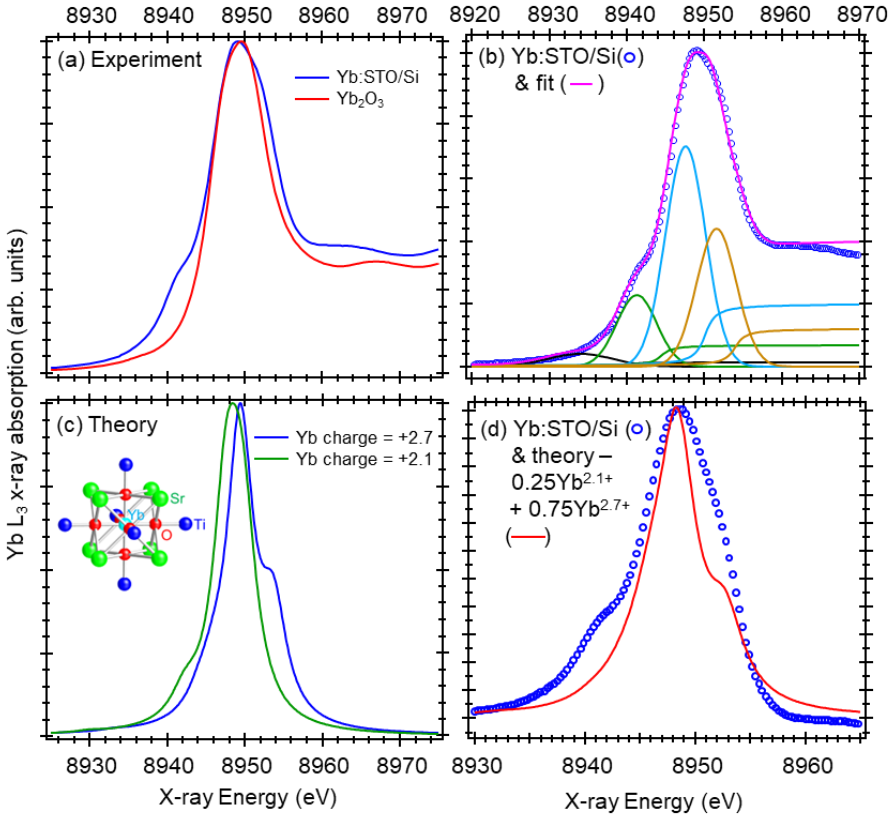

FIG 4 (a) Experimental Yb L_3-edge XANES for 12 nm $(Yb_{0.03},V_O):Sr_{0.97}TiO_{3-\delta}$/*i*-Si(001) and polycrystalline Yb_2O_3 powder. (b) A fit of the experimental spectrum for $(Yb_{0.03},V_O):Sr_{0.97}TiO_{3-\delta}$/*i*-Si(001) shown in panel (a) using Gaussians for the different features and arctan functions for the edge jumps associated with the different features. (c) Time-dependent density functional theory calculations of the Yb L_3-edge XANES for Yb substitution for Ti at the B-sites in STO assuming formal Yb charges of 2+ and 3+ which converge to values of 2.7+ and 2.1+ based on the quantum cluster shown in the inset. (d) Comparison of the experimental Yb L_3-edge XANES with a superposition of the two calculated spectra shown in panel (c) using weighting factors corresponding to 25% $Yb^{2.1+}$ and 75% $Yb^{2.7+}$.